

Orders of Recombination in Complete Perovskite Solar Cells – Linking Time-Resolved and Steady-State Measurements

Christian M. Wolff,^{*} Sean A. Bourelle, Le Quang Phuong, Jona Kurpiers, Sascha Feldmann, Pietro Caprioglio, Jose Antonio Marquez, Jakob Wolansky, Thomas Unold, Martin Stolterfoht, Safa Shoaee, Felix Deschler,^{*} and Dieter Neher^{*}

Ideally, the charge carrier lifetime in a solar cell is limited by the radiative free carrier recombination in the absorber which is a second-order process. Yet, real-life cells suffer from severe nonradiative recombination in the bulk of the absorber, at interfaces, or within other functional layers. Here, the dynamics of photogenerated charge carriers are probed directly in pin-type mixed halide perovskite solar cells with an efficiency >20%, using time-resolved optical absorption spectroscopy and optoelectronic techniques. The charge carrier dynamics in complete devices is fully consistent with a superposition of first-, second-, and third-order recombination processes, with no admixture of recombination pathways with non-integer order. Under solar illumination, recombination in the studied solar cells proceeds predominantly through nonradiative first-order recombination with a lifetime of 250 ns, which competes with second-order free charge recombination which is mostly if not entirely radiative. Results from the transient experiments are further employed to successfully explain the steady-state solar cell properties over a wide range of illumination intensities. It is concluded that improving carrier lifetimes to >3 μ s will take perovskite devices into the radiative regime, where their performance will benefit from photon-recycling.

1. Introduction

Lead halide perovskites and optoelectronic devices^[1] made thereof have attracted enormous attention due to a rapid rise in efficiency, the versatility of applications, and ease of processing. Concerted efforts in the development of perovskite solar cells have led to high photovoltaic and electroluminescent power conversion efficiencies of >20%,^[2–6] surpassing most single-junction thin-film solar cell technologies within just a decade after the initial demonstration. The performance of perovskite-based optoelectronic devices is limited by nonradiative decay processes which compete with radiative free carrier recombination. Therefore, detailed insights into the device operation and a detailed understanding of all recombination processes are imperative for further efficiency gains.

C. M. Wolff,^[+] J. Kurpiers, P. Caprioglio,^[++] J. Wolansky, M. Stolterfoht, D. Neher
Soft Matter Physics and Optoelectronics
Institute of Physics and Astronomy
University of Potsdam
Karl-Liebknecht-Str. 24-25, 14776 Potsdam, Germany
E-mail: christian.wolff@epfl.ch; neher@uni-potsdam.de

 The ORCID identification number(s) for the author(s) of this article can be found under <https://doi.org/10.1002/aenm.202101823>.

© 2021 The Authors. Advanced Energy Materials published by Wiley-VCH GmbH. This is an open access article under the terms of the Creative Commons Attribution License, which permits use, distribution and reproduction in any medium, provided the original work is properly cited.

^[+]Present address: École polytechnique fédérale de Lausanne STI IEM, Rue de la Maladière 71b, Neuchâtel 2000, Switzerland

^[++]Present address: Department of Physics, University of Oxford, Oxford, UK

^[+++]Present address: Walter Schottky Institut, Technische Universität München, Am Coulombwall 4, 85748 Garching, Germany

S. A. Bourelle, S. Feldmann, F. Deschler^[+++]
Cavendish Laboratory
Department of Physics
University of Cambridge
JJ Thomson Avenue, Cambridge CB3 0HE, UK
E-mail: felix.deschler@tum.de

L. Q. Phuong, J. Kurpiers, S. Shoaee
Optoelectronics of Disordered Semiconductors
Institute of Physics and Astronomy
University of Potsdam
Karl-Liebknecht-Str. 24-25, 14776 Potsdam, Germany

J. Kurpiers, P. Caprioglio
Helmholtz-Zentrum Berlin für Materialien und Energie
Young Investigator Group Perovskite Tandem Solar Cells
Kekuléstraße 5, 12489 Berlin, Germany

J. A. Marquez, T. Unold
Structure and Dynamics of Energy Materials
Helmholtz-Zentrum Berlin für Materialien und Energie
Hahn-Meitner-Platz 1, 14109 Berlin, Germany

DOI: 10.1002/aenm.202101823

The fate of photogenerated charges in neat perovskite layers has been extensively studied by time-resolved optical techniques including transient absorption spectroscopy (TAS),^[7–11] optical-pump-terahertz-probe (OPTP),^[12] time-resolved-microwave-conductivity (TRMC),^[13,14] time-resolved-photoluminescence (TRPL),^[15] time-resolved-2D-Fourier-transformed-infrared spectroscopy (TR-2D-FTIR)^[16] and other techniques. The results from these techniques have been explained by a superposition of first-, second, and third-order recombination processes:

$$R(n) = -\frac{dn}{dt} = k_1 \cdot n + k_{2,ext} \cdot n^2 + k_3 \cdot n^3 \quad (1a)$$

Here, n is the carrier density and R is the volume recombination rate. k_1 , $k_{2,ext}$ and k_3 are the coefficients for first-, second and third-order recombination processes, which are due to trap-assisted and surface recombination, direct band-to-band free carrier, and Auger recombination, respectively.^[17] Note that free carrier recombination causes the emission of photons,^[18] which may be reabsorbed. Therefore, $k_{2,ext}$ differs from the internal recombination coefficient $k_{2,int}$ (see below).

On the other hand, results from optoelectronic characterization techniques for full devices such as transient photovoltage (TPV), charge extraction (CE), or impedance spectroscopy (IS) have often been interpreted in terms of non-integer recombination order^[19,20]

$$R(n) = k_\alpha \cdot n^\alpha \quad (1b)$$

Such techniques commonly work in the small perturbation regime to measure the differential (small perturbation) lifetime τ defined via:^[21,22]

$$-\frac{d(\Delta n)}{dt} = R(n + \Delta n) - R(n) = \frac{dR}{dn} \Delta n \equiv \frac{\Delta n}{\tau} \quad (1c)$$

Here, τ is the characteristic decay time of the system back to the steady-state carrier population n after a short excitation to $n + \Delta n$. Obviously, it's only for neat first-order recombination that τ is independent of n . As shown in Figure S1 (Supporting Information), previous measurements on full devices yielded a density dependent τ corresponding to a recombination order α of typically >1 . While it is yet not clear which specific physical processes yield such non-integer recombination orders, we also note that the differential carrier lifetimes deduced from these measurements at a given carrier density differed significantly. For example, using methylammonium lead iodide, lifetimes ranging from μ s to ms have been reported from TMRC/TPV/IMVS under comparable excitation conditions.^[19,20,23–27] While such differences can be in part rationalized due to the manifold of recombination, extraction, and re-emission events that can happen in such multilayer devices, it was also noted that lifetimes from TPV and IS measurements are affected by capacitive contributions.^[28] Another complication arises from the fact that the external bias of an illuminated cell – and hence the effect of the electric fields on carrier distributions – may not properly reflect the conditions within the perovskite absorber,^[29] due to incomplete knowledge of unintentional doping and field-screening due to mobile ions in the perovskite absorber. Detailed knowledge of the recombination parameters and/or time constants is, however, required to rationalize the perfor-

mance of complete devices and identify avenues for improvements. Given the spread of reported recombination orders and carrier lifetimes in literature, a direct link between the dynamic processes on ns to μ s timescales and the device operation in steady-state is missing. The detailed knowledge of recombination parameters in operating devices would enable the precise identification of limiting processes or components for further device improvements toward 30% efficiency.^[30–32]

Here, we combine transient absorption spectroscopy and time-delayed-collection-field (TDCF^[33,34]) experiments on efficient perovskite devices to resolve the carrier recombination dynamics in fully operational devices. The unique combination of these two methods allowed us to cover a large range of carrier densities. The chosen techniques are free of ambiguous capacitance effects and work at a time range faster than the motion of ions in the perovskite layer. The analysis of these transient data revealed that free carrier recombination in the device at application-relevant conditions is entirely due to a first-order process. Non-integer order recombination but also a strong contribution of a nonradiative decay channel to second-order recombination could be safely ruled out. By complementing the results from these two techniques with steady-state photoluminescence and drift-diffusion simulations, we develop a fully descriptive model of the carrier dynamics in the devices and provide insight into the working principles of hybrid perovskite solar cells. Our comprehensive analysis quantifies recombination orders and velocities, carrier densities, and distributions, supported by simulations that reproduce the photovoltaic parameters under relevant operating conditions, enabling us to provide guidelines toward further efficiency gains.

2. Results

2.1. Sample Preparation

We prepared efficient p-i-n structured devices with a triple-cation-perovskite as the absorber layer (CsMAFA; CsI_{0.05}[FA_{0.85}MA_{0.15}Pb(I_{0.85}Br_{0.15})₃]_{0.95}) and organic p- and n-type charge transport layers (CTL; poly-triarylamine: PTAA and C₆₀).^[35] We also employ interlayers (PFN-P2 and LiF) at the perovskite|CTL interfaces for optimal performance.^[36–38] Figure 1A displays a cross-sectional SEM and corresponding schematic of a device. Devices are prepared with top electrode (Cu) thicknesses of either 100 nm for photovoltaic characterization and optoelectrical measurements or 20 nm for transient optical experiments in transmission (transient absorption in transmission mode). In Figure 1B,C we provide JV scans and EQE_{PV} spectra of the two device types, reaching efficiencies of $\approx 21\%$ with a V_{OC} of 1.165 V, a J_{SC} of 22.5 mA cm⁻², and a FF $\approx 80\%$. The devices with thinner electrodes exhibit reduced J_{SC} due to lower reflectivity of the back electrode and lower FF because of the higher series resistance of the thin Cu. The devices exhibit negligible hysteresis at varying scan speeds (Figure S2, Supporting Information), consistent with previous reports on low hysteresis in p-i-n devices with low recombination losses.^[39,40] The average V_{OC} is ≈ 25 mV lower in the semi-transparent device, which could stem from modifications in the optical stack, slightly lower carrier density and changed outcoupling efficiency due to the reduced back-electrode thickness.^[41,42]

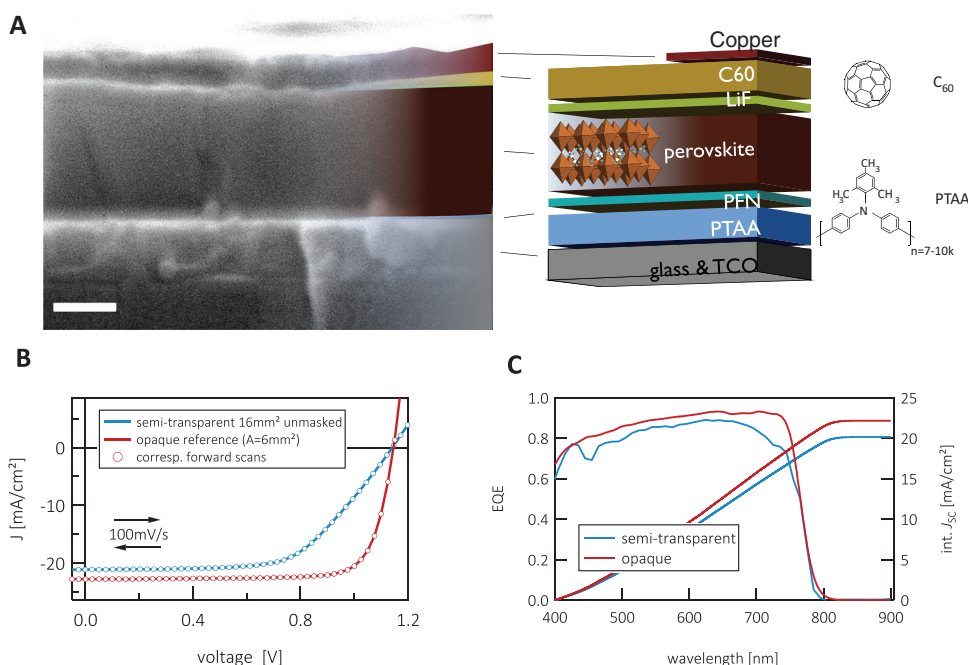


Figure 1. A) SEM cross-section and stack schematics of the p-i-n-type device architecture with the position of the individual layers (scale bar is 200 nm). Chemical structure of C₆₀ and PTAA. B) Typical *JV*-curves of the solar cells used in this study. Shown are an unmasked semi-transparent device (blue) and an opaque reference device (red) in forward (open circles) and backward (lines) scan direction at a scan rate of ≈ 100 mV s⁻¹. C) IPCE spectrum and integrated current (AM1.5G) of operating devices, delivering ≈ 22 mA cm⁻² (opaque) and ≈ 20 mA cm⁻² (semi-transparent).

2.2. Transient Absorption and Charge Extraction

In contrast to most previous studies, we performed the transient absorption experiments directly on operating devices. As described earlier, the devices for TAS had a semi-transparent top electrode with a sufficient transparency in the visible range >600 nm.^[43] The experiments are carried out at open-circuit with a background illumination ranging from 0.01 to 1 suns' equivalent to probe carrier dynamics under relevant operational conditions during real-world operation. In particular, background illumination will fill traps which could otherwise cause an initial decay of the free carrier density. Second, it reduces the internal electric field (compared to short circuit conditions) thereby reducing the rate of field-induced charge extraction during the delay between the pump and probe, which is particularly important for TDCF experiments at low carrier concentrations. We note that we observed a slight increase in carrier lifetime when increasing the background illumination density from 0.01 to 0.1 sun but then not further.

In **Figure 2A** we show the absorption and transient absorption signal. The TAS spectrum is dominated by a positive $\frac{\Delta T}{T}$ at ≈ 760 nm, which has been assigned to the ground-state-bleach due to the excitation of free carriers in the perovskite.^[11,44-46] The TAS experiments were performed with pulse fluences ranging between ≈ 10 and 1000 $\mu\text{J cm}^{-2}$. In this fluence range, the initial TAS signal depends linearly on fluence and can, therefore, be translated to a photogenerated charge-carrier concentration in the absorber layer^[9] (Figure S3a-d (Supporting Information) for further explanations and calibration, Figure S4 (Supporting Information) displays the shift between the derivative of the EQE and the PL, further accentuating that the signal does not stem from stimulated emission. The transient bleach

signal was hence converted to its corresponding carrier density and one set is shown in **Figure 2B**. At high fluence, an initial fast decay of the signal is indicative of higher-order recombination. The course of the transients becomes more similar below $n \approx 10^{17}$ cm⁻³, indicating the transition to a regime governed by first-order recombination.

One disadvantage of TAS is its limited sensitivity. This renders it difficult to sense carrier densities below 10^{16} cm⁻³ with a high enough signal-to-noise level. We, therefore, complemented our TAS measurements with a detailed investigation of the carrier dynamics using TDCF. A schematic of the TDCF setup is shown in **Figure 2C** (see the Supporting Information for a detailed description of the TDCF measurement scheme). In a TDCF experiment, charge carriers are photogenerated while the devices are held at a given pre-bias V_{pre} . After a given delay time, the carriers which survived recombination are extracted from the device by applying a reverse bias V_{coll} . The technique has been used in the past to study free charge generation and recombination in organic,^[34] inorganic^[47] and hybrid devices.^[48] A fluence series is shown in **Figure 2D** (see Figures S5 and S6 (Supporting Information) for additional data). The high sensitivity of an electrical probe in TDCF allowed us to follow the fate of the photogenerated charge carriers for fluences as low as 30 nJ cm⁻² and to carrier densities as small as 10^{14} cm⁻³. While the higher fluence transients show evidence for a higher-order recombination process, the low fluence transients exhibit the very same course meaning that the charge carrier decay proceeds exclusively due to a first-order recombination process. Unfortunately, recombination losses during charge extraction become visibly above a fluence of ≈ 2 $\mu\text{J cm}^{-2}$ ($n > 4 \times 10^{16}$ cm⁻³, as clearly seen in **Figure S3d** (Supporting Information), limiting the dynamic range of the TDCF experiments. Below that

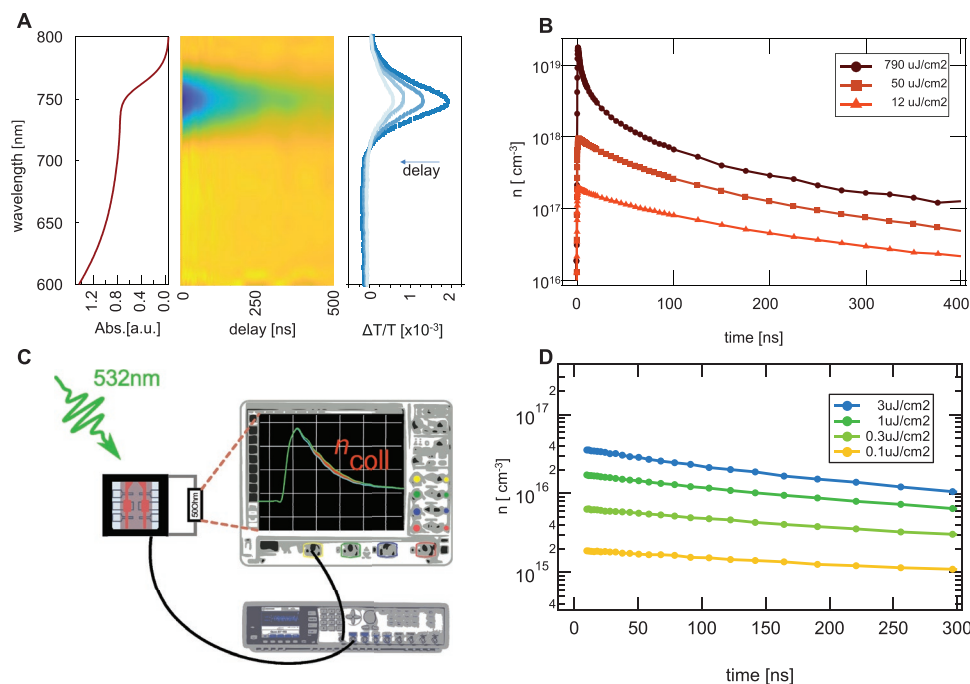


Figure 2. A) Absorption curve of a typical CsMAFA film, false color plot of the transient absorption spectra and cross sections thereof at the varying delay times. B) Transient ground-state-bleach traces converted to carrier density from TAS. C) Schematic of the TDCF setup. The solar cells are excited with a laser pulse while it is held at a given pre-bias ($=V_{OC}$). After a set delay, the function generator switches to reverse bias ($=V_{coll}$) and extracts the remaining charge. D) Extracted carrier density from TDCF for the indicated fluences. The measurements in B & D were conducted with 0.1 sun background illumination.

fluence, initial carrier densities from TDCF and TAS lie on one line and are strictly linear in fluence.

In the case that the recombination dynamics depend only on the carrier density (and not on the excitation history), transients measured under different initial carrier concentrations can be overlaid by shifting the transients in the time-domain, regardless of the initial carrier concentration and delay time after photoexcitation. This is exactly shown in **Figure 3A**, where we merge the photoinduced carrier density as a function of the delay time from TAS and TDCF, with the fluence varying over five orders of magnitude (see Figure S6 (Supporting Information) for the full set of experiments under different background illumination intensities). This first result is important in two aspects: 1) it shows that the devices do not change their behavior – through, e.g., degradation – even if exposed to high irradiance over the time of measurement and 2) that there is a single set of intrinsic recombination parameters that describes the decay of the charge carrier population. Both techniques reveal consistently a mono-exponential decay at low densities and an accelerated decay from higher carrier concentrations $>10^{16} \text{ cm}^{-3}$.

We extract the recombination order from the time derivative of the measured carrier density kinetics –, i.e., dn/dt – as shown in Figure 3B (see the Supporting Information regarding the analysis of the TDCF transients). We find that the entire set of data can be well fitted by a superposition of first-, second-, and third-order recombination processes (solid blue line) according to Equation (1a). The colored regions in Figure 3B indicate the carrier density regimes in which first-, second- and third order processes dominate. The value of k_3 corresponds to an upper limit, as we didn't reach a clear n^3 - dominated (Auger-) regime due to the $>$ nanosecond time resolution of our setup.

The region of dominant second-order recombination is resolved in both TAS and TDCF data, yielding an external second-order recombination coefficient $k_{2,ext} \approx 3 \times 10^{-11} \text{ cm}^3 \text{ s}^{-1}$. To check whether the presence of the transporting layers and the electrodes accelerates the second-order recombination in full devices we performed TAS measurements on a neat perovskite layer on glass, with the result shown in Figure S7 (Supporting Information). Second-order interfacial recombination has been proposed recently.^[49] Within the accuracy of the experiment, the high fluence recombination properties of the neat perovskite layer and the full device stack lay on top of each other, ruling out any significant effect of the internal interfaces of the device on the second-order recombination properties. Fitting the recombination data of the film with pure second-order recombination yields $k_{2,ext}(\text{film}) = 3 \pm 0.3 \times 10^{-11} \text{ cm}^3 \text{ s}^{-1}$, in close agreement to the full device. We actually expected a slightly smaller value for $k_{2,ext}(\text{film})$. As pointed out above, $k_{2,ext}$ differs from the internal (local) recombination coefficient $k_{2,int}$ due to the reabsorption of photons by the active layer. For pure radiative recombination, $k_{2,ext} = p_{em} \cdot k_{2,int}$, where p_{em} is the probability of photon outcoupling.^[18,50–52] We have determined $p_{em} = 7.3\%$ by simulating the full device structure with flat interfaces as outlined in the corresponding Supplementary Note. This is close to the simple estimate $p_{em} \approx 1/2n_r^2$ (with $n_r = 2.5$ the refractive index of the perovskite). As both approaches neglect additional outcoupling by scattering at grain boundaries and due to surface roughness, these estimates are lower limits. Setting $p_{em} = 8\%$, yields $k_{2,int} = 3.8 \times 10^{-10} \text{ cm}^3 \text{ s}^{-1}$. For the flat neat layer, our calculation in the Supplementary Note yields an outcoupling efficiency for the flat neat layer of $p_{e,flat} = 6.5\%$. However, the difference

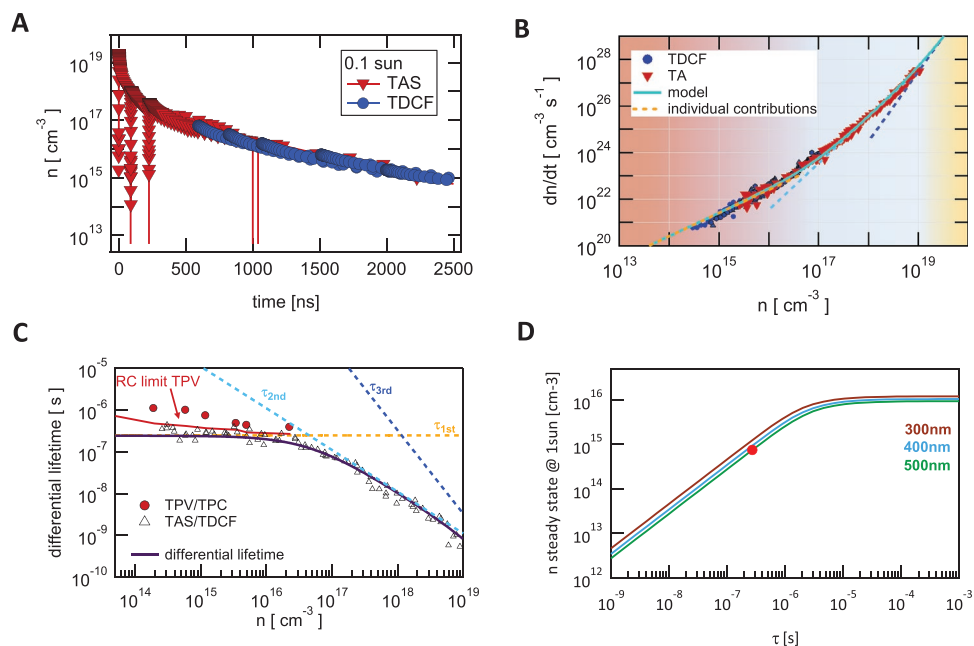


Figure 3. A) Transient charge carrier dynamics under 0.1 sun equivalent background illumination. TAS (red) and TDCF (blue) are performed on full devices at V_{OC} . B) Temporal derivative of (A), showing three ranges with first-, second-, and third-order dominated regimes and the individual contributions with the background coloration. Additionally shown is the modelled recombination rate as a function of carrier density (light blue) and guides-to-the-eye of the first-, second- and third order (dashed lines). C) Differential lifetimes deduced from the $R(n)$ data in Figure 3b according to Equation (1c) (triangles) and from TPV (red circles) as a function of carrier density. The red line shows the limit for TPV measurements according to Kiermasch et al.,^[28] the solid line shows the numerical derivative of the total fit (purple) and the dashed lines the corresponding contributions as denoted. The resolution limit is at $\approx 1\text{--}2$ ns. D) Carrier concentration versus nonradiative lifetime $\tau = k_1^{-1}$ for three different thicknesses (fixed generation of $= 2.9 \times 10^{21} \text{ cm}^{-3} \text{ s}^{-1}$) as calculated with Equation (1a) using the values of k_2 and k_3 listed in Table 1 with a data point indicating the device in this study (red dot).

to $p_{e,dev.}$ ($= 7.3\%$) is too small to cause a resolvable difference in the experimental data.

The linear region covers the range below $n \approx 1 \times 10^{16} \text{ cm}^{-3}$, with $k_1 = 4 \times 10^6 \text{ s}^{-1}$. It has been shown that second-order recombination of photogenerated charge with background recombination causes an apparent first-order recombination.^[53] We argue in the Supporting Information that this effect is small even for 1 sun background illumination. Also, we show below that the density of doping-induced charges is no more than 10^{13} cm^{-3} , which is much smaller than the photogenerated carrier density in our transient experiment. We conclude that recombination at low carrier density is due to a true first-order processes, with a density-independent carrier lifetime $\tau = k_1^{-1} = 250 \text{ ns}$. We finally note that the steady-state recombination rate at V_{OC} under simulated solar illumination is $R_{1sun} = G_{1sun} = J_{SC}/(q \cdot d) = 2.9 \times 10^{21} \text{ cm}^{-3} \text{ s}^{-1}$. According to the data in Figure 3B, higher order effects can be safely excluded at this recombination rate, meaning that our cell under working condition are dominated by strict first-order recombination. There is abandoned evidence that the carrier lifetime in full devices is governed by recombination at and across the interface between the perovskite and the adjacent charge transporting layers.^[31,32,37,54]

Figure 3C plots the differential lifetime as deduced from the (n) data in Figure 3b with Equation (1c). In the high carrier density regime ($n > 10^{16} \text{ cm}^{-3}$), the lifetimes deduced from our combined TDCF/TAS measurements are inversely proportional to the carrier density. This regime is dominated by second-order recombination, where $\tau \approx (2 \cdot k_{2,ext} \cdot n)^{-1}$. At densities below 10^{16} cm^{-3} , the lifetime values become independent of

carrier concentration, meaning that the fate of photogenerated carriers in this regime is entirely determined by a first-order recombination process ($\tau \approx k_1^{-1}$). As noted earlier, TPV/CE measurements are popular techniques to determine carrier recombination lifetimes in devices under operational conditions. Results from such measurements on our devices are plotted by full circles in Figure 3D. In contrast to the TAS/TDCF data, the lifetimes from TPV/CE increase with decreasing carrier density according to a non-integer recombination order of ≈ 1.7 . It's only within a small range of carrier densities ($10^{15} - 10^{16} \text{ cm}^{-3}$) that lifetimes are similar for all techniques. Higher lifetimes and non-integer recombination orders seem to be common for many electrical measurements on full devices (Figure S1, Supporting Information). Related to this, reported carrier lifetimes in devices are generally larger than in neat perovskite layers at the same carrier density, particularly when considering low carrier densities, as mentioned in the introduction. This can in part be attributed to an experimental limitation (solid red line, $\tau_{cap.} = \frac{nk_B T}{q} \times \frac{C}{J_{0,rad.}} \times e^{qV_{oc}/nk_B T}$) of the employed methods, i.e., the resistance-capacitance (RC) time of the devices, as shown by Kiermasch et al.^[28] In contrast to TPV/CE, our TDCF/TAS data reveal a constant lifetime $\tau = k_1^{-1} = 250 \text{ ns}$, which we assign to nonradiative first-order recombination.

2.3. Linking Transient and Steady-State Results

Having quantified the kinetic parameters for the main recombination processes in our solar cells, we aim to establish a direct

link between the dynamic processes and steady-state device operation. Using the results from TAS and TDCF, we can calculate the charge carrier densities under steady-state conditions by numerically solving Equation (1a) with a constant generation rate G . With $G_{1sun} = 2.9 \times 10^{21} \text{cm}^{-3}\text{s}^{-1}$ under simulated solar illumination, we find a steady-state carrier concentration of $n_{1sun} = (7.3 \pm 0.3) \times 10^{14} \text{cm}^{-3}$. On the other hand, an intrinsic carrier density of $n_i \cong 1.25 \times 10^5 \text{cm}^{-3}$ is estimated from the radiative dark recombination current $J_{0,rad} = 3 \times 10^{-24} \text{A cm}^{-2}$ (Figure S8, Supporting Information) under the assumption of radiative second-order recombination with an external recombination coefficient of $k_{2,ext} \cong 3 \times 10^{-11} \text{cm}^3 \text{s}^{-1}$ (see Supplementary Note). From these two densities, we predict a Quasi-Fermi level splitting ($QFLS$) in the perovskite bulk of 1.166 eV which agrees with the measured V_{OC} . We have shown earlier that cells comprising PTAA and C_{60} CTLs exhibit a slow enough recombination at the internal interfaces to not cause a significant bending of the $QFLS$ of the majority carriers near the charge extracting contact, justifying the approximation $qV_{OC} = QFLS$.^[29] Notably, our estimate of the carrier density under AM1.5 G illumination is almost one order of magnitude lower than in previous reports.^[19,20,24,55] But even if the recombination was only second-order, i.e., $G = R = k_{2,ext} n^2$, the carrier density would not exceed $9 \times 10^{15} \text{cm}^{-3}$ and any improvement in light outcoupling (enhancing $k_{2,ext}$) will actually reduce the internal carrier density in the radiative limit.^[56] Johnston and Herz numerically predicted a maximum $n_{1sun} = 6 \times 10^{15} \text{cm}^{-3}$ if SRH recombination is slow ($\tau_{SRH} > 10 \mu\text{s}$). Figure 3D shows n_{1sun} calculated from our experimentally obtained $k_1, k_{2,ext}, k_3$ for varying nonradiative lifetimes between 1 ns and 1 ms. The carrier concentration saturates for $\tau_1 > 10 \mu\text{s}$ at a value of $8 \times 10^{15} \text{cm}^{-3}$ for an absorber thickness of 300 – 500 nm. That number poses an upper limit,

since any additional recombination (e.g., due to interfacial or trap recombination) or extraction would reduce the carrier density even further. This is exactly the case in our devices where recombination at internal interfaces but also SRH recombination in the bulk reduces the steady-state concentration.

Though the simple model reproduces the steady-state experimental data accurately, it relies on the assumption of equal and constant electron and hole densities across the perovskite, which is an approximation in a real device, where charge extraction to the ETL and HTL may depopulate selectively one carrier reservoir locally while injected charges drift into the active layer. We, therefore, simulated the steady-state device by employing drift-diffusion simulations (SCAPS).^[29] To account for surface recombination, we translated the measured nonradiative first-order lifetimes into a surface recombination velocity S through Equation (2),

$$k_1 = \frac{1}{\tau} = \frac{1}{\tau_{bulk}} + \left(\frac{4d^2}{\pi^2 D} + \frac{d}{S} \right)^{-1} \quad (2)$$

where τ_{bulk} is the bulk lifetime (800 ns), d the active layer thickness (480 nm), D the electron/hole diffusion coefficient ($2 \text{cm}^2 \text{s}^{-1}$). Notably, other combinations of surface recombination velocities yield similar results w.r.t. the final k_1 with similar device properties. All other parameters were taken from the analysis of the data from the analytic model (see the right column in Table 1) and from our previous work on bilayers.^[37,57] We acknowledge that SCAPS does not consider the presence of mobile ions in the perovskite layers. It has been shown that ion motion in combination with surface recombination may have a substantial influence on the device properties.^[39] As discussed earlier and shown in Figure S2 (Supporting Information),

Table 1. Measured values and values of different parameters as obtained from the application of the dynamic model (Equation (1)) and of SCAPS drift-diffusion simulations to the experimental data. Values in parentheses were determined experimentally and kept constant in the dynamic model and/or the SCAPS drift-diffusion (DD) simulations.

	Measurement ^{a)}	dynamic model	DD simulation
k_1^{-1} (ns)	250 ± 60	250 ± 60	$800 + S_{1/2} = 150 / 50 \text{cm s}^{-1}$
$k_{2,ext}$ ($\text{cm}^3 \text{s}^{-1}$)	$2.9 \pm 0.4 \times 10^{-11}$	$2.9 \pm 0.4 \times 10^{-11}$	(3×10^{-11})
k_3 ($\text{cm}^6 \text{s}^{-1}$)	10^{-30}	10^{-30}	(10^{-30})
p_0 (cm^{-3})	–	$1.1 \pm 0.5 \times 10^{13}$	(10^{13})
n_{1sun} (cm^{-3})	–	$7.2 \pm 0.3 \times 10^{14}$	$5\text{--}7.5 \times 10^{14}$, slightly imbalanced
$J_{0,rad}$ (A m^{-2})	$3.0 \pm 0.2 \times 10^{-20}$	$3.0 \pm 0.2 \times 10^{-20}$	–
n_i^2 (cm^{-6})	–	$1.6 \pm 0.2 \times 10^{10}$	–
E_G (eV)	1.61 ± 0.02	–	(1.6)
$N_C N_V$ (cm^{-6})	–	$1.0 \pm 0.3 \times 10^{37}$	$(1 \times 10^{37} = (3.3 \times 10^{18})^2)$
m^*/m_e	–	0.25 ± 0.03	–
d (nm)	480 ± 15	–	–
PLQY (%)	0.33 ± 0.05	0.43 ± 0.06	0.38

^{a)}The inverse first-order recombination coefficient k_1^{-1} , the external second-order recombination coefficient $k_{2,ext}$ and the Auger recombination coefficient k_3 ($\text{cm}^6 \text{s}^{-1}$) are determined from the fit of the experimental decay data in Figure 3D to the rate equation Equation (1) with $G = 0$. The background doping density was determined from the low-intensity plateau of the PLQY in Figure 4C. The steady-state carrier density under 1 sun illumination conditions, n_{1sun} , is calculated with the dynamic model based on the measured recombination parameters and a generation rate of $G = 2.9 \times 10^{21} \text{cm}^{-3} \text{s}^{-1}$ or deduced from DD simulations. From these values, the dark radiative recombination current density, $J_{0,rad}$, the intrinsic carrier density, n_i^2 , the product of the effective state density in the conduction and valance band, N_C and N_V , respectively, and the effective mass, m^* , are calculated as outline in the Supporting Information 2. Finally, d is the device thickness, and PLQY the external quantum efficiency of photoluminescence.

our devices exhibit a small hysteresis in the measured scan speed range, however, that does not rule out that the internal field gets partially screened by rapidly moving ions. On the other hand, we and others have recently shown that the influence of ions on the *JV* properties becomes largely suppressed for reduced interface recombination.^[30,58] Also, simulations with SCAPS gave good fits to *JV* and $V_{OC}(I)$ data of devices with even higher values of *S* as reported here, using similar input parameters.^[30] The simulation of the *JV* curves of one of our present devices with the above parameters is shown in **Figure 4A** while **Figure 4B** shows the simulated carrier profile in the device. At open circuit and one sun illumination, the carrier profile is slightly imbalanced, but the average value agrees well with the aforementioned carrier density of $\approx 7 \cdot 10^{14} \text{cm}^{-3}$. As charge carrier recombination under 1 sun conditions is dominated by recombination at the perovskite-TL interface, the fairly constant carrier density implies that charge carriers can diffuse throughout the entire layer at a faster rate than they recombine at the interfaces. This raises the question of whether device operation is significantly affected by the electric field across the active layer.^[59] To address this, we performed simulations where the relative dielectric constant of the perovskite was varied by two orders of magnitude, from 10 to 1000 (the main simulations here use $\epsilon_r = 22$) to screen the internal electric field (see Figures S9 and S10: Supporting Information). The effect of increasing ϵ_r (screening the internal field) becomes apparent above $\epsilon_r \approx 10$, from which on the FF (PCE) drops from 83% to 77% (21.8% to 20%). As such, our devices likely benefit slightly from an internal field, assisting charge extraction, but the effect

is rather weak. Note that field screening may also originate from mobile ions, but our simulations suggest an only weak effect on the overall performance of our devices.

Intensity dependent measurements of the external quantum efficiency of PL, PLQY, is a powerful approach to investigate the mechanism of charge recombination^[60,61]. In **Figure 4C**, our experimental values for the PLQY are shown versus intensity. These experiments have been performed on complete devices with electrodes attached at V_{OC} . The data is compared to the PLQY calculated based on

$$PLQY = \frac{(k_{2,ext} - k_{2,nr}) \cdot n \cdot (n + p_0)}{k_1 \cdot n + k_{2,ext} \cdot n \cdot (n + p_0) + k_3 \cdot n^3} \quad (3)$$

Within a small confidence interval – indicated by the grey area – the modelled values (blue line) agree with the measured data. Note that in Equation (3), we included a nonradiative second-order contribution, $k_{2,nr}$. In recent studies, a nonradiative second-order recombination coefficient was discussed^[9,41,62] but the origin of this contribution is yet unclear.^[63] On the other hand, Davies et al. showed that second-order recombination in a neat methylammonium lead triiodide perovskite layer is the inverse of the absorption process^[18] and obeys the van Roosbroeck-Shockley relation.^[64] Also, external luminescence efficiencies above 50% have been reported for mixed halide perovskites, suggesting an only small contribution by nonradiative second-order recombination.^[65–67] In the intensity range covered in **Figure 4C**, $PLQY \approx (k_{2,ext} - k_{2,nr}) \cdot (n + p_0) / k_1$. With

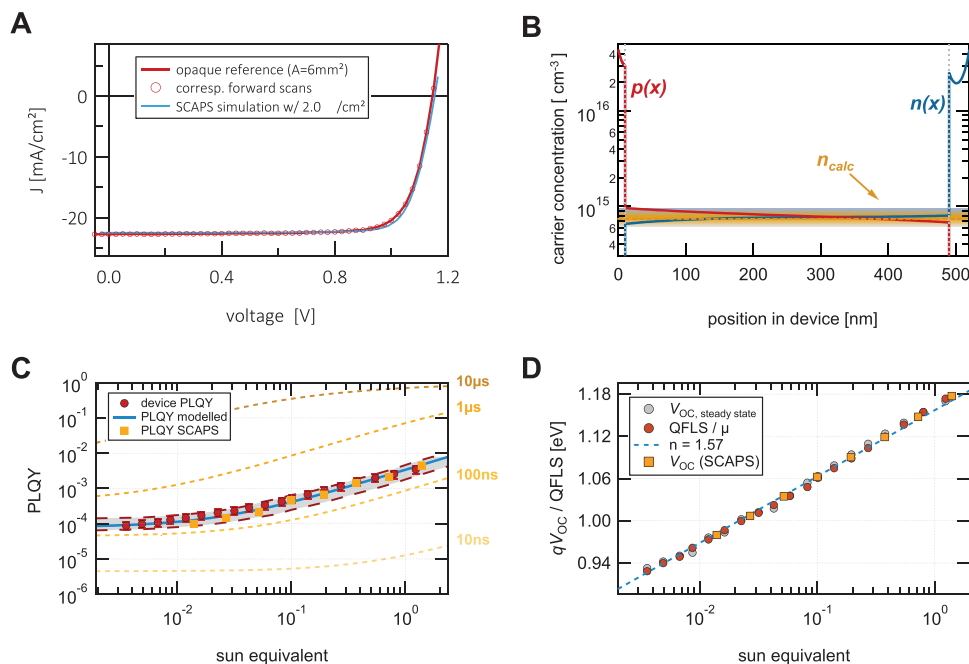


Figure 4. A) Measured (red, at a scan rate of 120 mV s^{-1}) and simulated *JV*-scans (blue). B) Carrier profiles (electrons – blue, holes – red) from the SCAPS simulation in panel A at 1 sun and open-circuit. Within a small error margin (orange shading), the carrier density in the bulk agrees very well with the value of $0.75 \times 10^{15} \text{ cm}^{-3}$ (orange) as estimated from our simplified rate model. C) PLQY measurements (red circles) on full devices. The kinetic model (light blue) with an error band (grey) explains the measured values reasonably well and the PLQY obtained from SCAPS simulations (orange) are consistent. In orange shadings, we show PLQY values expected for the indicated nonradiative lifetimes when keeping $k_{2,ext}$, and p_0 constant. D) Open circuit voltage as a function of light intensity, measured in the device (grey), extracted from PLQY (i.e., QFLS, red), calculated from SCAPS (orange), and additionally a line indicating an ideality factor of 1.57 (blue).

k_1 and $k_{2,ext}$ taken from your transient experiments, we estimate $k_{2,nr} < 0.9 \cdot 10^{-11} \text{cm}^3 \text{s}^{-1}$ within the error margin of our fits (see Figure S11 in the Supporting Information). A nonradiative $k_{2,nr}$ contributing considerably to the measured $k_{2,ext}$ would reduce the emitted photon flux and with that the PLQY well below the measured values.

We also introduced a doping density $p_0 = 1.1 \cdot 10^{13} \text{cm}^{-3}$, which contributes to radiative recombination to explain the plateau at intensities below 0.01 suns adequately. This value is in agreement with recent findings on mixed perovskites.^[66] Notably, the actual doping density could be higher without impacting the overall recombination dynamics significantly below a threshold of $p_0 < k_1/k_2 \approx 10^{17} \text{cm}^{-3}$. This poses an upper limit because of the comparably low lifetimes in the full devices (i.e., recombination is dominated by $k_1 > k_{2,ext}p_0$). This is in accord with results by Yavari and Ebadi et al.^[68] The authors artificially doped the perovskite (likewise triple cation perovskite) with >10 ppm heterovalent Bi^{3+} atoms. With a unit cell volume of $\approx 1 \text{ nm}^3$ this corresponds to a doping density of 10^{16}cm^{-3} , which in turn already reduces the TRPL lifetime by roughly twofold. The result of DD simulations with SCAPS is shown with solid yellow squares in Figure 4C,D. As the simulation also considers the carrier density profile in the device, the simulated PLQY follows the measured PLQY even more closely above 0.1 suns. Figure 4D displays the measured V_{OC} in comparison with the QFLS as calculated from the PLQY according to $QFLS = k_B T \cdot \ln(PLQY \times J_{SC}/J_{0,rad})$ and the result of DD simulations. The simulation provides a good prediction of the V_{OC} over two orders of magnitude, which highlights the accuracy and consistency of our model.

For 1 sun illumination intensity, we measure for our solar cells a PLQY of 0.33%, close to the calculated value of 0.4% (0.38% obtained from SCAPS). Plotted in Figure S12A (Supporting Information) is the predicted PLQY as a function of τ_{SRH} together with a literature survey. We further estimated the internal PLQY of the samples with $PLQY_{int.} = PLQY_{ext.}/[p_{em.} + (1 - p_{em.} - p_{par.})PLQY_{ext.}] = 3.8\%$ at 1 sun, while assuming parasitic absorption to be negligible (i.e., $p_{par.} = 0$).^[69] With such fairly high internal PLQYs, the question arises whether the open-circuit is impacted by photon-recycling. We calculate that the improvement in open-circuit voltage at such PLQEs is minor < 10 mV (Figure S12B, Supporting Information). Increasing the minority carrier lifetime only by a threefold to $\approx 1 \mu\text{s}$ should allow an additional gain of 20 mV and for lifetimes exceeding 3 μs this gain could then be also preserved when reducing the carrier density, as is the case at the operating point (i.e., MPP) so that actual efficiency gains are possible.

3. Conclusion

In conclusion, we show that the charge carrier recombination dynamics in efficient p-i-n-type perovskite solar cells can be described as a superposition of first-, second-, and third-order recombination, without the necessity to introduce a non-integer recombination order. We find that the kinetic variables $k_1 \approx 4 \cdot 10^6 \text{s}^{-1}$, $k_{2,ext.} \approx 3 \cdot 10^{-11} \text{cm}^3 \text{s}^{-1}$, $k_3 \leq 1 \cdot 10^{-30} \text{cm}^6 \text{s}^{-1}$, and a background doping density of $p_0 \approx 10^{13} \text{cm}^{-3}$ fully describe device operation. Numerically solving the rate equation

$dn/dt = G - k_1 \cdot n - k_{2,ext.} \cdot n \cdot (n + p_0) - k_3 \cdot n^3$ allows us to calculate a steady-state carrier density $< 10^{15} \text{cm}^{-3}$ under 1 sun. With the obtained rate constants and carrier densities, we reproduce external luminescent efficiencies and the open-circuit voltage of the devices over several orders of magnitude, without the need to introduce a significant nonradiative second-order recombination pathway. When employing drift-diffusion simulations, the measured and experimentally determined JV characteristics agree and the simulations reveal fairly homogenous carrier profiles throughout the active layer at open-circuit. Our results suggest that prototypical devices with open-circuit voltages below 1.2 V (at a bandgap of $\approx 1.6 \text{ eV}$) operate in the nonradiative regime, but on the verge of the radiative regime. Slight improvements in a nonradiative lifetime to $> 1 \mu\text{s}$ in the device will be sufficient to enter the radiative regime and benefit from photon-recycling. Optical management to enhance the emission at the band-edge of the perovskite will further enhance luminescent outcoupling, and enable higher photovoltages in return.

Supporting Information

Supporting Information is available from the Wiley Online Library or from the author.

Acknowledgements

In memory of John A. Love. The authors acknowledge help by Stresing Entwicklungsbüro, specifically G. Stresing for assistance with the TAS spectrometers, F. Jaiser for general lab assistance, F. Dornack, A. Pucher, A. Horka, and B. Stiller for technical assistance. Funding was provided by HyPerCells (a joint graduate school of the Potsdam University and the HZB), PoGS (Potsdam Graduate School), as well as the Deutsche Forschungsgemeinschaft (DFG, German Research Foundation) within the SPP2196 (SURPRISE 423749265). Further, S.B., S.F. and F.D. acknowledge funding from the EPSRC (Doctoral Prize Fellowship, S.F.), the Studienstiftung des Deutschen Volkes (S.F.), as well as support from the DFG Emmy Noether Program (F.D., 387651688) and the Winton Programme for the Physics of Sustainability. S.S. and L.Q.P. thank the Alexander von Humboldt Foundation for funding. C.M.W. thanks for funding through Marie Skłodowska Curie fellowship, grant agreement no. 101033077 and L. Kegelmann, S. Albrecht, T. Kirchartz for fruitful discussions.

Open access funding enabled and organized by Projekt DEAL.

Conflict of Interest

The authors declare no conflict of interest.

Author Contributions

C.M.W., F.D. and D.N. planned the experiments that were carried out by C.M.W., S.A.B., S.F., and L.Q.P. C.M.W. carried out the analysis of the data and simulations with SCAPS with help from P.C. and M.S. J.A.M.P. and T.U. contributed to simulations of the PLQY and photon-recycling. T.U., F.D., and D.N. supervised the work. C.M.W. wrote the manuscript with input from all co-authors.

Data Availability Statement

Data available on request from the authors.

Keywords

carrier lifetimes, interfacial recombination, perovskite solar cells, recombination dynamics, time resolved spectroscopy

Received: June 14, 2021
Revised: September 20, 2021
Published online:

- [1] C. Zuo, H. J. Bolink, H. Han, J. Huang, D. Cahen, L. Ding, *Adv. Sci.* **2016**, 3, 1500324.
- [2] M. A. Green, Y. Hishikawa, E. D. Dunlop, D. H. Levi, J. Hohl-Ebinger, M. Yoshita, A. W. Y. Ho-Baillie, *Prog. Photovoltaics Res. Appl.* **2019**, 27, 3.
- [3] Y. Cao, N. Wang, H. Tian, J. Guo, Y. Wei, H. Chen, Y. Miao, W. Zou, K. Pan, Y. He, H. Cao, Y. Ke, M. Xu, Y. Wang, M. Yang, K. Du, Z. Fu, D. Kong, D. Dai, Y. Jin, G. Li, H. Li, Q. Peng, J. Wang, W. Huang, *Nature* **2018**, 562, 249.
- [4] J. J. Yoo, G. Seo, M. R. Chua, T. G. Park, Y. Lu, F. Rotermund, Y.-K. Kim, C. S. Moon, N. J. Jeon, J.-P. Correa-Baena, V. Bulović, S. S. Shin, M. G. Bawendi, J. Seo, *Nature* **2021**, 590, 587.
- [5] J. Jeong, M. Kim, J. Seo, H. Lu, P. Ahlawat, A. Mishra, Y. Yang, M. A. Hope, F. T. Eickemeyer, M. Kim, Y. J. Yoon, I. W. Choi, B. P. Darwich, S. J. Choi, Y. Jo, J. H. Lee, B. Walker, S. M. Zakeeruddin, L. Emsley, U. Rothlisberger, A. Hagfeldt, D. S. Kim, M. Grätzel, J. Y. Kim, *Nature* **2021**, 592, 381.
- [6] Y. Hassan, J. H. Park, M. L. Crawford, A. Sadhanala, J. Lee, J. C. Sadighian, E. Mosconi, R. Shivanna, E. Radicchi, M. Jeong, C. Yang, H. Choi, S. H. Park, M. H. Song, F. De Angelis, C. Y. Wong, R. H. Friend, B. R. Lee, H. J. Snaith, *Nature* **2021**, 591, 72.
- [7] S. D. Stranks, G. E. Eperon, G. Grancini, C. Menelaou, M. J. P. Alcocer, T. Leijtens, L. M. Herz, A. Petrozza, H. J. Snaith, *Science* **2013**, 342, 341.
- [8] G. Xing, N. Mathews, S. Sun, S. S. Lim, Y. M. Lam, M. Gratzel, S. Mhaisalkar, T. C. Sum, *Science* **2013**, 342, 344.
- [9] J. M. Richter, M. Abdi-Jalebi, A. Sadhanala, M. Tabachnyk, J. P. H. Rivett, L. M. Pazos-Outón, K. C. Gödel, M. Price, F. Deschler, R. H. Friend, *Nat. Commun.* **2016**, 7, 13941.
- [10] Y. Yang, M. Yang, Z. Li, R. Crisp, K. Zhu, M. C. Beard, *J. Phys. Chem. Lett.* **2015**, 6, 4688.
- [11] J. S. Manser, P. V. Kamat, *Nat. Photonics* **2014**, 8, 737.
- [12] C. Wehrenfennig, M. Liu, H. J. Snaith, M. B. Johnston, L. M. Herz, *Energy Environ. Sci.* **2014**, 7, 2269.
- [13] E. M. Hutter, G. E. Eperon, S. D. Stranks, T. J. Savenije, *J. Phys. Chem. Lett.* **2015**, 6, 3082.
- [14] C. Mombblona, L. Gil-Escrig, E. Bandiello, E. M. Hutter, M. Sessolo, K. Lederer, J. Blochwitz-Nimoth, H. J. Bolink, *Energy Environ. Sci.* **2016**, 9, 3456.
- [15] F. Staub, H. Hempel, J.-C. Hebig, J. Mock, U. W. Paetzold, U. Rau, T. Unold, T. Kirchartz, *Phys. Rev. Appl.* **2016**, 6, 044017.
- [16] A. a. Bakulin, O. Selig, H. J. Bakker, Y. L. a. Rezus, C. Müller, T. Glaser, R. Lovrincic, Z. Sun, Z. Chen, A. Walsh, J. M. Frost, T. L. C. Jansen, *J. Phys. Chem. Lett.* **2015**, 6, 3663.
- [17] L. M. Herz, *Annu. Rev. Phys. Chem.* **2016**, 67, 65.
- [18] C. L. Davies, M. R. Filip, J. B. Patel, T. W. Crothers, C. Verdi, A. D. Wright, R. L. Milot, F. Giustino, M. B. Johnston, L. M. Herz, *Nat. Commun.* **2018**, 9, 293.
- [19] S. Wheeler, D. Bryant, J. Troughton, T. Kirchartz, T. Watson, J. Nelson, J. R. Durrant, *J. Phys. Chem. C* **2017**, 121, 13496.
- [20] D. Kiermasch, P. Rieder, K. Tvingstedt, A. Baumann, V. Dyakonov, *Sci. Rep.* **2016**, 6, 39333.
- [21] J. Bisquert, F. Fabregat-Santiago, I. Mora-Seró, G. Garcia-Belmonte, S. Giménez, *J. Phys. Chem. C* **2009**, 113, 17278.
- [22] C. G. Shuttle, B. O'Regan, A. M. Ballantyne, J. Nelson, D. D. C. Bradley, J. de Mello, J. R. Durrant, *Appl. Phys. Lett.* **2008**, 92, 093311.
- [23] J.-P. Correa-Baena, W. Tress, K. Domanski, E. H. Anaraki, S.-H. Turren-Cruz, B. Roose, P. P. Boix, M. Grätzel, M. Saliba, A. Abate, A. Hagfeldt, *Energy Environ. Sci.* **2017**, 10, 1207.
- [24] Y. Shao, Y. Yuan, J. Huang, *Nat. Energy* **2016**, 1, 15001.
- [25] I. Zarazúa, S. Sidhik, T. López-Luke, D. Esparza, E. De la Rosa, J. Reyes-Gomez, I. Mora-Seró, G. Garcia-Belmonte, *J. Phys. Chem. Lett.* **2017**, 8, 6073.
- [26] I. Zarazua, G. Han, P. P. Boix, S. Mhaisalkar, F. Fabregat-Santiago, I. Mora-Seró, J. Bisquert, G. Garcia-Belmonte, *J. Phys. Chem. Lett.* **2016**, 7, 5105.
- [27] I. Gelmetti, N. F. Montcada, A. Pérez-Rodríguez, E. Barrena, C. Ocal, I. García-Benito, A. Molina-Ontoria, N. Martín, A. Vidal-Ferran, E. Palomares, *Energy Environ. Sci.* **2019**, 12, 1309.
- [28] D. Kiermasch, A. Baumann, M. Fischer, V. Dyakonov, K. Tvingstedt, *Energy Environ. Sci.* **2018**, 11, 629.
- [29] P. Caprioglio, M. Stolterfoht, C. M. Wolff, T. Unold, B. Rech, S. Albrecht, D. Neher, *Adv. Energy Mater.* **2019**, 9, 1901631.
- [30] J. Diekmann, P. Caprioglio, M. H. Futscher, V. M. Le Corre, S. Reichert, F. Jaiser, M. Arvind, L. P. Toro, E. Gutierrez-Partida, F. Peña-Camargo, C. Deibel, B. Ehrler, T. Unold, T. Kirchartz, D. Neher, M. Stolterfoht, *Sol. RRL* **2021**, 5, 2100219.
- [31] J. Wang, W. Fu, S. Jariwala, I. Sinha, A. K.-Y. K. Y. Jen, D. S. Ginger, *ACS Energy Lett.* **2019**, 4, 222.
- [32] S. Jariwala, S. Burke, S. Dunfield, R. C. Shallcross, M. Taddei, J. Wang, G. E. Eperon, N. R. Armstrong, J. J. Berry, D. S. Ginger, *Chem. Mater.* **2021**, 33, 5035.
- [33] J. Kniepert, M. Schubert, J. C. Blakesley, D. Neher, *J. Phys. Chem. Lett.* **2011**, 2, 700.
- [34] J. Kurpiers, T. Ferron, S. Roland, M. Jakoby, T. Thiede, F. Jaiser, S. Albrecht, S. Janietz, B. A. Collins, I. A. Howard, D. Neher, *Nat. Commun.* **2018**, 9, 2038.
- [35] M. Saliba, J.-P. Correa-Baena, C. M. Wolff, M. Stolterfoht, N. Phung, S. Albrecht, D. Neher, A. Abate, *Chem. Mater.* **2018**, 30, 4193.
- [36] M. Stolterfoht, P. Caprioglio, C. M. Wolff, J. A. Márquez Prieto, J. Nordmann, S. Zhang, D. Rothhardt, U. Hörmann, Y. Amir, A. Redinger, L. Kegelmann, F. Zu, S. Albrecht, N. Koch, T. Kirchartz, M. Saliba, T. Unold, D. Neher, J. A. Márquez, J. Nordmann, S. Zhang, D. Rothhardt, U. Hörmann, Y. Amir, A. Redinger, L. Kegelmann, F. Zu, S. Albrecht, N. Koch, T. Kirchartz, M. Saliba, T. Unold, D. Neher, *Energy Environ. Sci.* **2019**, 12, 2778.
- [37] M. Stolterfoht, C. M. Wolff, J. A. Márquez, S. Zhang, C. J. Hages, D. Rothhardt, S. Albrecht, P. L. Burn, P. Meredith, T. Unold, D. Neher, *Nat. Energy* **2018**, 3, 847.
- [38] C. M. Wolff, F. Zu, A. Paulke, L. P. Toro, N. Koch, D. Neher, *Adv. Mater.* **2017**, 29, 1700159.
- [39] P. Calado, A. M. Telford, D. Bryant, X. Li, J. Nelson, B. C. O'Regan, P. R. F. Barnes, *Nat. Commun.* **2016**, 7, 13831.
- [40] P. Lopez-Varo, J. A. Jiménez-Tejada, M. García-Rosell, S. Ravishanker, G. Garcia-Belmonte, J. Bisquert, O. Almora, *Adv. Energy Mater.* **2018**, 8, 1702772.
- [41] F. Staub, T. Kirchartz, K. Bittkau, U. Rau, *J. Phys. Chem. Lett.* **2017**, 8, 5084.
- [42] I. L. Braly, D. W. DeQuilettes, L. M. Pazos-Outón, S. Burke, M. E. Ziffer, D. S. Ginger, H. W. Hillhouse, *Nat. Photonics* **2018**, 12, 355.
- [43] B. Chen, Y. Bai, Z. Yu, T. Li, X. Zheng, Q. Dong, L. Shen, M. Boccard, A. Gruverman, Z. Holman, J. Huang, *Adv. Energy Mater.* **2016**, 6, 1601128.
- [44] J. C. Brauer, Y. H. Lee, M. K. Nazeeruddin, N. Banerji, *J. Phys. Chem. Lett.* **2015**, 6, 3675.

- [45] Y. Yang, D. P. Ostrowski, R. M. France, K. Zhu, J. van de Lagemaat, J. M. Luther, M. C. Beard, *Nat. Photonics* **2015**, *10*, 53.
- [46] M. B. Price, J. Butkus, T. C. Jellicoe, A. Sadhanala, A. Briane, J. E. Halpert, K. Broch, J. M. Hodgkiss, R. H. Friend, F. Deschler, *Nat. Commun.* **2015**, *6*, 8420.
- [47] J. Kurpiers, D. M. Balazs, A. Paulke, S. Albrecht, I. Lange, L. Protesescu, M. V. Kovalenko, M. A. Loi, D. Neher, *Appl. Phys. Lett.* **2016**, *108*, 103102.
- [48] A. Paulke, S. D. Stranks, J. Kniepert, J. Kurpiers, C. M. Wolff, N. Schön, H. J. Snaith, T. J. K. Brenner, D. Neher, *Appl. Phys. Lett.* **2016**, *108*, 113505.
- [49] E. T. Roe, K. E. Egelhofer, M. C. Lonergan, *ACS Appl. Energy Mater.* **2018**, *1*, 1037.
- [50] L. M. Pazos-Outon, M. Szumilo, R. Lamboll, J. M. Richter, M. Crespo-Quesada, M. Abdi-Jalebi, H. J. Beeson, M. Vru ini, M. Alsari, H. J. Snaith, B. Ehrler, R. H. Friend, F. Deschler, *Science* **2016**, *351*, 1430.
- [51] W.-A. Quitsch, D. W. deQuilettes, O. Pfingsten, A. Schmitz, S. Ognjanovic, S. Jariwala, S. Koch, M. Winterer, D. S. Ginger, G. Bacher, *J. Phys. Chem. Lett.* **2018**, *9*, 2062.
- [52] T. W. Crothers, R. L. Milot, J. B. Patel, E. S. Parrott, J. Schlipf, P. Müller-Buschbaum, M. B. Johnston, L. M. Herz, *Nano Lett.* **2017**, *17*, 5782.
- [53] G. F. A. Dibb, T. Kirchartz, D. Credgington, J. R. Durrant, J. Nelson, *J. Phys. Chem. Lett.* **2011**, *2*, 2407.
- [54] B. Das, Z. Liu, I. Aguilera, U. Rau, T. Kirchartz, *Mater. Adv.* **2021**, *2*, 3655.
- [55] D. Kiermasch, L. Gil-Escrig, A. Baumann, H. J. Bolink, V. Dyakonov, K. Tvingstedt, *J. Mater. Chem. A* **2019**, *7*, 14712.
- [56] O. D. Miller, E. Yablonovitch, S. R. Kurtz, *IEEE J. Photovoltaics* **2012**, *2*, 303.
- [57] P. Caprioglio, C. M. Wolff, O. J. Sandberg, A. Armin, B. Rech, S. Albrecht, D. Neher, M. Stollerfoht, *Adv. Energy Mater.* **2020**, *10*, 2000502.
- [58] N. Wu, D. Walter, A. Fell, Y. Wu, K. Weber, *J. Phys. Chem. C* **2020**, *124*, 219.
- [59] O. J. Sandberg, J. Kurpiers, M. Stollerfoht, D. Neher, P. Meredith, S. Shoaee, A. Armin, *Adv. Mater. Interfaces* **2020**, *7*, 2000041.
- [60] S. D. Stranks, V. M. Burlakov, T. Leijtens, J. M. Ball, A. Goriely, H. J. Snaith, *Phys. Rev. Appl.* **2014**, *2*, 34007.
- [61] S. Draguta, J. A. Christians, Y. V. Morozov, A. Mucunzi, J. S. Manser, P. V. Kamat, J. M. Luther, M. Kuno, *Energy Environ. Sci.* **2018**, *11*, 960.
- [62] T. Kirchartz, F. Staub, U. Rau, *ACS Energy Lett.* **2016**, *1*, 731.
- [63] F. Staub, U. Rau, T. Kirchartz, *ACS Omega* **2018**, *3*, 8009.
- [64] W. van Roosbroeck, W. Shockley, *Phys. Rev.* **1954**, *94*, 1558.
- [65] D. W. deQuilettes, S. Koch, S. Burke, R. K. Paranj, A. J. Shropshire, M. E. Ziffer, D. S. Ginger, *ACS Energy Lett.* **2016**, *1*, 438.
- [66] S. Feldmann, S. Macpherson, S. P. Senanayak, M. Abdi-Jalebi, J. P. H. Rivett, G. Nan, G. D. Tainter, T. A. S. S. Doherty, K. Frohna, E. Ringe, R. H. Friend, H. Sirringhaus, M. Saliba, D. Beljonne, S. D. Stranks, F. Deschler, *Nat. Photonics* **2020**, *14*, 123.
- [67] M. Abdi-Jalebi, Z. Andaji-Garmaroudi, S. Cacovich, C. Stavrakas, B. Philippe, J. M. Richter, M. Alsari, E. P. Booker, E. M. Hutter, A. J. Pearson, S. Lilliu, T. J. Savenije, H. Rensmo, G. Divitini, C. Ducati, R. H. Friend, S. D. Stranks, *Nature* **2018**, *555*, 497.
- [68] M. Yavari, F. Ebadi, S. Meloni, Z. S. Wang, T. C. J. Yang, S. Sun, H. Schwartz, Z. Wang, B. Niesen, J. Durantini, P. Rieder, K. Tvingstedt, T. Buonassisi, W. C. H. Choy, A. Filippetti, T. Dittrich, S. Olthof, J. P. Correa-Baena, W. Tress, *J. Mater. Chem. A* **2019**, *7*, 23838.
- [69] T. Kirchartz, J. A. Márquez, M. Stollerfoht, T. Unold, *Adv. Energy Mater.* **2020**, *10*, 1904134.